Investigation of thermal management for lithium-ion pouch battery module based on phase change slurry and mini channel cooling plate

Bai, Fanfei; Chen, Mingbiao; Song, Wenji; Yu, Qinghua; Li, Yongliang; Feng, Ziping; Ding, Yulong

DOI:
10.1016/j.energy.2018.10.137

Document Version
Peer reviewed version

Citation for published version (Harvard):
Bai, F, Chen, M, Song, W, Yu, Q, Li, Y, Feng, Z & Ding, Y 2019, 'Investigation of thermal management for lithium-ion pouch battery module based on phase change slurry and mini channel cooling plate', *Energy*, vol. 167, pp. 561-574. https://doi.org/10.1016/j.energy.2018.10.137

Accepted Manuscript

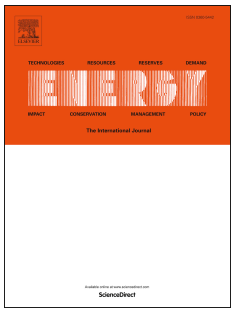

Investigation of thermal management for lithium-ion pouch battery module based on phase change slurry and mini channel cooling plate

Fanfei Bai, Mingbiao Chen, Wenji Song, Qinghua Yu, Yongliang Li, Ziping Feng, Yulong Ding

PII: S0360-5442(18)32132-7

DOI: https://doi.org/10.1016/j.energy.2018.10.137

Reference: EGY 14034

To appear in: *Energy*

Received Date: 4 September 2018

Revised Date: 19 October 2018

Accepted Date: 23 October 2018

Please cite this article as: Bai F, Chen M, Song W, Yu Q, Li Y, Feng Z, Ding Y, Investigation of thermal management for lithium-ion pouch battery module based on phase change slurry and mini channel cooling plate, *Energy* (2018), doi: https://doi.org/10.1016/j.energy.2018.10.137.

Investigation of thermal management for lithium-ion pouch battery module based on phase change slurry and mini channel cooling plate

Fanfei Bai,[a,b,c,d,e] Mingbiao Chen,[a,b,c] Wenji Song,[a,b,c]* Qinghua Yu,[e] Yongliang Li,[e]* Ziping Feng,[a,b,c] Yulong Ding[e]

[a]Guangzhou Institute of Energy Conversion, Chinese Academy of Sciences, Guangzhou 510640, China

[b]CAS Key Laboratory of Renewable Energy, Chinese Academy of Sciences, Guangzhou 510640, China

[c]Guangdong Provincial Key Laboratory of New and Renewable Energy Research and Development, Guangzhou 510640, China

[d]University of Chinese Academy of Sciences, Beijing 10049, China

[e]School of Chemical Engineering, University of Birmingham, Birmingham B15 2TT, United Kingdom

The following are the e-mails of the authors:

1) Name: Fanfei Bai E-mail: baiff@ms.giec.ac.cn

2) Name: Mingbiao Chen E-mail: chenmb@ms.giec.ac.cn

3) Name: Wenji Song* E-mail: songwj@ms.giec.ac.cn

4) Name: Qinghua Yu E-mail: Q.Yu@bham.ac.uk

5) Name: Yongliang Li* E-mail: y.li.1@bham.ac.uk

6) Name: Ziping Feng E-mail: fengzp@ms.giec.ac.cn

7) Name: Yulong Ding E-mail: Y.Ding@bham.ac.uk

Highlights：

- Battery thermal management based on the PCS and mini channel was proposed.
- The cooling plate was designed to balance the cooling effect and energy consumption.
- The management cooled battery effectively and performed better than water cooling.
- The optimal mass flow rate for different concentrations of PCS was determined.
- The dimensionless empirical formulas were obtained.

Abstract： In this paper, the thermal management based on phase change slurry (PCS) and mini channel cooling plate for the lithium-ion pouch battery module was proposed. The three-dimensional thermal model was established and the optimum structure of the cooling plate with mini channel was designed with the orthogonal matrix experimental method to balance the cooling performance and energy consumption. The simulation results showed that the cooling performance of PCS consisting of 20% n-octadecane microcapsules and 80% water was better than that of pure water, glycol solution and mineral oil, when the mass flow rate was less than 3 ×

10^{-4} kg s^{-1}. For different concentrations of PCS, if the mass flow rate exceeded the critical value, its cooling performance was worse than that of pure water. When the cooling target for battery maximum temperature was higher than 309 K, the PCS cooling with appropriate microcapsule concentration had the edge over in energy consumption compared with water cooling. At last, the dimensionless empirical formula was obtained to predict the effect of the PCS's physical parameters and flow characteristics on the heat transfer and cooling performance. The simulation results will be useful for the design of PCS based battery thermal management systems.

Keywords：Phase change slurry; Cooling plate; Battery thermal management; Dimensionless empirical formula

Nomenclature

t time (s)

T_{max} maximum temperature (K)

T_{min} minimum temperature (K)

ΔT_{max} maximum temperature difference (K)

ΔT temperature difference (K)

T_0 ambient temperature (K)

T temperature (K)

θ excess temperature (K)

θ_{max} maximum excess temperature (K)

θ_{max0} maximum excess temperature without cooling (K)

ΔP pressure drop (Pa)

P static pressure (Pa)

c_p specific heat (J kg^{-1} K^{-1})

ρ density (kg m^{-3})

λ thermal conductivity (W m^{-1} K^{-1})

λ' effective thermal conductivity (W m^{-1} K^{-1})

q heat (W)

U open-circuit voltage (V)

V terminal voltage (V)

I current (A)

A area (m^2)

d diameter (m)

L latent heat (J kg^{-1})

h heat transfer coefficient (W m^{-2} K^{-1})

V volume (m^3)

$\dot{m}$ mass flow rate (kg s^{-1})

∇ nabla operator

u velocity (m s^{-1})

μ apparent viscosity (m^2 s^{-1})

$\vec{V}$	velocity vector
$\vec{f}$	fluid volume force vector
$\vec{F}_{viscous}$	fluid viscous force vector
C	constant
C_v	volume fraction
C_m	mass concentration
y	core-to-shell weight ratio
e	shear rate
Gr	Grashof number
Nu	Nusselt number
Pr	Prandtl Number
Re	Reynolds number
Pe	Peclet number
Θ	excess temperature dimensionless number
n	number of cooling channels
w	total width of cooling channels (mm)
δ	thickness of cooling channels (mm)

Subscripts

bat	battery
out	outlet
in	inlet
Al	aluminum
X	X direction
Y	Y direction
Z	Z direction
v	volume
m	mass
p	particle
c	core
s	shell
f	carrier fluid

Acronyms

HEV	hybrid electric vehicle
EV	electric vehicle
PCM	phase change material
PCS	phase change slurry
mPCM	micro-encapsulated PCM
BTMS	battery thermal management system
SOC	state of charge

1. Introduction

Lithium-ion batteries made from multiple cells connected parallel have been targeted for use in electric vehicles (EVs) and hybrid electric vehicles (HEVs) due to their high power capability and energy density[1]. The thermal safety risk of large capacity lithium battery module is improved as battery module with more energy can be released during a single cell failure[2]. The battery thermal management system (BTMS) is used to limit the maximum temperature (T_{max}) of battery

module during normal operation in order to avoid thermal runaway and also to decrease the maximum temperature difference (ΔT_{max}) to prolong the battery lifespan[3]. Many thermal management technologies for battery packs in EVs or HEVs have been developed in the past few decades, including air cooling, liquid cooling, phase change material (PCM) cooling and heat pipes cooling[4][5]. Besides, some innovative cooling technologies, such as boiling based cooling method[6][7] and couple multiple cooling method[8], are also developed.

As moving devices, like pumps or blowers, are not required, passive thermal management based on the PCM is more cost-effective and reliable[9]. The heat generated by the battery can be absorbed by the PCM located between the cells of battery modules. When the temperature of the cell reaches the PCM melting point, further heat will be stored in the PCM as latent heat with no further increase in temperature[10][11]. However, it is difficult to employ this method efficiently because of the relatively low thermal conductivity (< 0.5 W m^{-1} K^{-1}), which leads to a temperature gradient inside the PCM[12][13][14][15]. Furthermore, during the phase change process the PCM expands or shrinks, which may lead to leaking and an increase in thermal resistance. Most importantly, unlike with active thermal management, the BTMS based on the PCM cannot remove the heat in the PCM instantaneously to attain a sustained and effective cooling performance[16].

Liquid cooling technology has become the most widely used cooling technology in industrial applications. Compared with the PCM, liquid has higher thermal conductivity which leads to higher cooling performance and is more suitable for large-scale battery packs. Liu[17] concluded that the liquid cooling made the strongest cooling effect under a normal environment temperature condition and the Reynolds number influenced the effect of the liquid cooling performance greatly. The liquid cold plate with mini-channels, as a method of indirect cooling, was shown to be more

practical than direct liquid cooling though it had a slightly lower cooling performance[18][19][20]. The number of mini-channels and the inlet mass flow rate influence the T_{max} of the battery[21]. Additionally, the effect of discharge rates and operating temperature was investigated in the reference[22][23]. A novel BTMS based on PCM and water cooling plate was also designed to cool the pouch battery module [8]. The water cooling plate was employed in cooling the near-electrode area with a high heat generation rate. The PCM also played a role in absorbing the heat generated by other parts of the battery.

The phase change slurry (PCS) is made up of micro-encapsulated PCM (mPCM) and carrier fluid. The mPCM consists of PCM as core material and polymer as shell material[24]. PCS has high latent heat capacity and high energy density as it combines the properties of PCM with liquid coolant. It can store or release a large amount of heat at a relatively stable temperature and transfer the heat during the flow[25]. However, it is more difficult to pump compared with pure water, especially at low temperatures. The viscosity of PCS is 10 times higher than that of water when the mass concentration of mPCM is 30% and the temperature is 293 K[26]. While, the research of Delgado[27] indicated that when the fluid velocity is higher than 0.4 m s^{-1}, the pumping power of PCS is less than that of pure water for the same amount of heat removal. Moreover, a carefully selected concentration of mPCM could effectively reduce the flow rate and reduce the total pumping power[28]. Compared with water and PCM, the advantage of PCS in energy conservation and temperature control was further demonstrated in an under-floor electric heating system and floor cooling system[29][30]. The heat transfer in the melting region was highly enhanced by the use of PCS in a micro channel under constant heat flux[31]. Although, the use of PCS for heat storage or heat transfer was widely investigated[32][33], research on the use of PCS in battery cooling is still

limited. Zhang[34] used n-octadecane ($C_{18}H_{37}$) and pentadecane ($C_{15}H_{31}$) as the heat transfer media of the PCS cycle for EV battery cooling and heating, respectively. A comparison with direct cabin air blow and refrigerant circulation methods using 1st Law and 2nd Law analysis showed that the PCS cycle method had higher energy efficiency.

In conclusion, as the PCS combines the outstanding convection heat transfer effect of the liquid cooling technology and the advantage of the latent heat in heat storage, it can play an important role in battery cooling. In order to ensure the superiority of the BTMS based on the PCS, the cooling performance of the PCS in a battery module should be investigated and the results will be compared with the water cooling performance. And the simulation results can be used as a reference for the arrangement of experimental scheme and the engineering application. In this paper a PCS based on water and n-octadecane microcapsules was used in a mini channel cooling plate to restrain the rise in battery temperature and attain a more uniform temperature field. The study focused on the cooling performance of the PCS in a battery module. The orthogonal experiment method was used to optimize the structure design of the mini channel cooling plate with PCS. Furthermore, the cooling performance of the PCS was compared with that of other liquids. The effect of mPCM's melting point, concentration as well as the mass flow rate of PCS on the cooling performance was studied. Lastly, the simulation results were dealt with dimensionless method and an empirical formula was derived to describe the effect of the PCS's physical parameters and flow characteristics on the heat transfer and cooling performance.

2. Model

2.1 Physical problem

The combination of mini-channel cooling plate and PCS was used to reduce the T_{max} and the ΔT_{max} of the battery. The cooling plates with mini channels were set between adjacent batteries, as shown in Fig. 1. The width and height of the cooling plate equals to that of the pouch battery. The PCS flowed into the mini channel inlet near the electrode area and removed the battery heat generated. The mini channels were straight and uniformly distributed in order to decrease the pressure drop (ΔP) of PCS and improve the uniformity of the temperature field. The number, total width and thickness of cooling channel (the size of the cooling channels in the X directions, as the Fig.1 shows) in the cooling plate would be validated and optimized to obtain better heat dissipation. The physical sizes and thermal properties used in the simulation are summarized in Table 1. T_0 is the ambient temperature. X, Y and Z denote the size of the module in orthogonal directions, respectively.

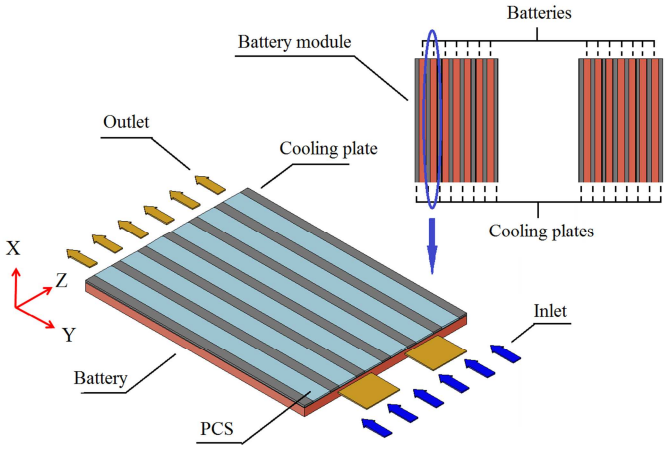

Fig. 1 The structure of battery module and cooling plate

GAMBIT was used to mesh the model and FLUENT 17 was used as the simulation software. The transient solver was used to simulate the cooling performance of the battery in discharging mode. The inlet and outlet conditions of the simulation were the inlet velocity and outlet pressure. As the maximum Reynolds number of the PCS was less than 2300, the laminar flow model was

chosen. The environment temperature, the initial temperature of the batteries and the inlet temperature of the PCS were set to 300 K. In order to simplify the cost of calculation, the theoretical model was developed based on the following assumptions:

(1) The mPCM was assumed evenly distributed in the PCS.

(2) The specific heat of mPCM in liquid and solid phase was constant.

(3) The volume of the mPCM was constant during the phase change process.

(4) The PCS was assumed to be incompressible.

The independent test of grid number and time step were performed to guarantee accuracy. The mesh with 896199 grids and a time step of 0.1 s were used in the simulation. The convergence criteria for flow and energy were set to 10^{-6}.

Table 1 Specifications and parameters of the battery and cooling plate

Parameters	Value	Parameters	Value
Nominal capacity (Ah)	20	Al foil thickness (mm)	0.02
Nominal voltage (V)	3.25	Anode thickness (mm)	0.08
Size (mm)	230×170×7	Cathode thickness (mm)	0.07
Weight (g)	545	Separator thickness (mm)	0.03
Maximum discharge current (A)	40	Thermal conductivity along surfaces (W m^{-1} K^{-1})	12 [8]
Discharge operating temperature (K)	253-333	Thermal conductivity in thickness direction (W $m^{-1}K^{-1}$)	0.34 [8]
Anode material	$LiPFeO_4$	Average battery specific heat (J kg^{-1} K^{-1})	2138 [8]
Cathode material	Li_xC_6	Wall thickness of cooling plate (mm)	0.5
Separator	PE/PP/PP	Aluminum thermal conductivity (W m^{-1} K^{-1})	202.4 [21]
Electrolyte	$LiPF_6$	Aluminum specific heat (J kg^{-1} K^{-1})	871 [21]
Cu foil thickness (mm)	0.01	Aluminum density (kg m^{-3})	2719 [21]

2.2 Governing equations

2.2.1. Thermal model of the battery

The energy conservation of a battery follows:

$$\rho_{bat} c_{p,bat} \frac{\partial T}{\partial t} = \lambda_{bat} \nabla^2 T + q_{bat} \quad (1)$$

where ρ_{bat}, $c_{p,bat}$, λ_{bat}, and q_{bat} are the density, specific heat capacity, thermal conductivity and heat generation of battery, respectively. T is temperature and t is the time.

The heat generation of the battery was different because of the different size, type and discharging rate. When the Li-ion battery operated at working conditions, the relationship between heat generation and electrical parameters can be written as following [2]:

$$q_{bat} = I(U - V) - I(T \frac{dU}{dT}) \quad (2)$$

where U, V and I is the open circuit voltage, terminal voltage and current of battery, respectively. In this paper, a uniform battery heat generation based on an electro-thermal coupled model for the pouch battery in the previous work was used[35]. To verify the battery heat generation model, the experiment and simulation results of temperature and voltage were compared, respectively. In the experiment, the 20Ah LiFePO4/C pouch battery was used. In the thermostat, the battery was charged with 1/3 C constant current then 3.65 V constant voltage. Here, the discharge rate C is equal to discharge current divided by the nominal capacity. After resting for 1 hour, the battery was discharged with constant-current (CC) to 2.9 V. The discharge rate was 0.5 C, 1.0 C, 1.5 C and 2 C, respectively. There were 6 T-type thermocouples distributed on the battery surface to monitor the battery temperature. An image of the experimental set-up and a comparison of the experimental and simulation values follows:

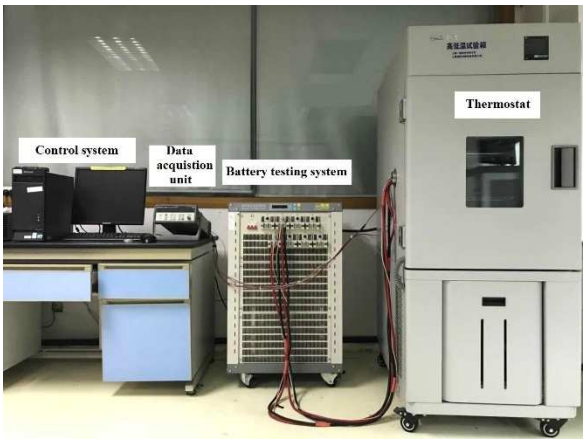

(a)

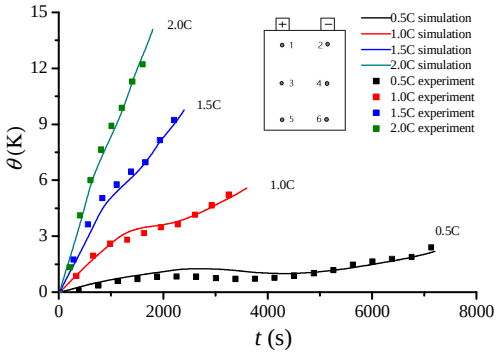

(b)

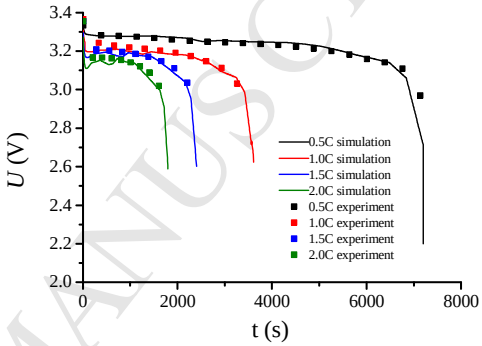

(c)

Fig. 2 (a) An image of the experimental set-up, (b) mean temperature of 6 points on the battery surface, (c) voltage versus discharging time

In the module, the heat removed by the PCS, q_{PCS}, is calculated as:

$$q_{PCS} = c_{p,PCS}\rho_{PCS}u_{PCS}A_{in}(T_{out} - T_{in}) \tag{3}$$

where $c_{p,PCS}$, u_{PCS} and ρ_{PCS} are the specific heat, velocity and density of the PCS, respectively. The qualitative temperature is the mean value of the inlet temperature T_{in} and the outlet temperature T_{out}. A_{in} is the inlet area of the mini channel.

The energy conservation equation, the momentum conservation equation and the continuity equation of the PCS in the mini channel are given as follows:

$$\rho c_p \frac{\partial T}{\partial t} + \rho c_p u \cdot \nabla T + \nabla \cdot (-\lambda \nabla T) = q \tag{4}$$

$$\frac{\partial \vec{V}}{\partial t} + (\vec{V} \cdot \nabla)\vec{V} = -\frac{1}{\rho}\nabla P + \vec{f} + \frac{1}{\rho}\vec{F}_{viscous} \tag{5}$$

$$\frac{\partial \rho}{\partial t} + \nabla \cdot (\rho u) = 0 \tag{6}$$

where $\vec{V}$, $\vec{f}$, $\vec{F}_{viscous}$ represent the velocity vector, volume force vector and viscous force vector, respectively. And P is the static pressure.

The surface heat transfer conditions is not taken into account since the liquid cooling has a much stronger effect on heat transfer than the natural convection and radiant heat transfer.

2.2.2 Governing equation of the physical properties of mPCM and PCS

Mass concentration of the mPCM in the PCS is an important parameter. As the mass concentration increases, both the heat capacity and the viscosity of the slurry increase while the thermal conductivity decreases. All these will influence the performance of heat transfer. The volume fraction, C_v, depends on the density and mass concentration C_m. And it can be described as Eq. (7):

$$C_v = C_m \frac{\rho_{PCS}}{\rho_p} \tag{7}$$

where the subscripts p and PCS mean particle and PCS, respectively, and C_v and C_m indicate the volume fraction and mass concentration, respectively.

According to the law of conservation of mass, the density of mPCM can be calculated by the densities of core/shell materials and the ratio of core to the shell:

$$\rho_p = \frac{(1+y)\rho_c\rho_s}{\rho_c + y\rho_s} \tag{8}$$

where the subscripts c and s indicate core and shell, respectively, and y is the core to shell weight ratio. During the phase change process, the density of core material will change by 10 - 15%. As the core material concentration in the bulk slurry is low, the change in slurry density is no more than 3%. So the density of slurry can be treated as a constant[36]. Thus, the density of PCS can be

calculated as in Eq. (9):

$$\rho_{PCS} = \frac{\rho_p \rho_f}{C_m \rho_f + (1 - C_m)\rho_p} \tag{9}$$

where the subscript *f* refers to the carrier fluid.

The specific heat of mPCM and PCS can be calculated as relation (10-11):

$$c_{p,p} = \frac{(y c_{p,c} + c_{p,s})\rho_c \rho_s}{(\rho_c + y\rho_s)\rho_p} \tag{10}$$

$$c_{p,PCS} = C_m c_{p,p} + (1 - C_m) c_{p,f} \tag{11}$$

The specific heat of the liquid and solid phase may be assumed as constant as the concentration of mPCM is low[37].

The thermal conductivity of the mPCM can be calculated by the composite sphere approach:

$$\frac{1}{\lambda_p d_p} = \frac{1}{\lambda_c d_c} + \frac{d_p - d_c}{\lambda_s d_p d_c} \tag{12}$$

$$\left(\frac{d_c}{d_p}\right)^3 = \frac{\rho_s}{\rho_s + y\rho_c} \tag{13}$$

where d_p and d_c refer to the particle and core diameters, respectively.

The thermal conductivity of the PCS is calculated as in relation (14)：

$$\lambda_{PCS} = \lambda_f \frac{2\lambda_f + \lambda_p + 2C_v(\lambda_p - \lambda_f)}{2\lambda_f + \lambda_p - C_v(\lambda_p - \lambda_f)} \tag{14}$$

Because of the interaction between fluid and mPCM, the actual thermal conductivity become higher when the PCS flows. The effective thermal conductivity can be written as follows[38]:

$$\frac{\lambda_{PCS}^{'}}{\lambda_{PCS}} = 1 + BC_v Pe_p^n \tag{15}$$

where $\lambda_{PCS}^{'}$ is the effective thermal conductivity of the PCS.

Pe_p is the particle Peclet number defined as[39]:

$$Pe_p = \frac{ed^2}{\alpha_f} \tag{16}$$

where e is the shear rate, a_f is the thermal diffusivity of carrier fluid, and values of B and n depend on the particle Peclet number:

$$\begin{cases} B = 3.0 & n=1.5 & Pe_P < 0.67 \\ B = 1.8 & n=0.18 & 0.67 \le Pe_P \le 250 \\ B = 3.0 & n=1/11 & Pe_P > 250 \end{cases} \tag{17}$$

The viscosity of PCS has important implications on the pressure drop (ΔP) and power consumption when it is used to transport energy. Higher viscosity leads to higher ΔP, which means higher power consumption. As the temperature falls or the mass concentration rises, the viscosity of the PCS increases. The apparent viscosity of the slurry can be calculated as in Eq. (18)

$$\frac{\mu_{PCS}}{\mu_f} = (1 - C_v - NC_v^2)^{-2.5} \tag{18}$$

where N is a parameter which is related to the size, shape, rigidity and type of the mPCM and can be obtained experimentally. For a particle diameter of 6.3 μm, the N is 1.16[40].

As the optimum temperature range of the battery was 298 - 313 K[41], it was appropriate that the phase change temperature of the mPCM used in the battery thermal management was in the range of 303 - 308 K. The mPCM used in the simulation was prepared by the ultrasonic-assisted mini

emulsion in-situ polymerization[42]. The shell and the core of the mPCM were polystyrene and n-octadecane, respectively. The mPCM was uniformly distributed in the water to prepare the PCS used in the simulation. The properties of the materials used in the PCS are shown in Table 2.

Table 2 Properties of material used in the PCS[43].

Item	n-octadecane	Polystyrene	Water
ρ (kg m^{-3})	814	1050	998.2
c_p (J kg^{-1} K^{-1})	1900	1300	4182
λ (W m^{-1} K^{-1})	0.21	0.08	0.6
υ (kg m^{-1} s^{-1})	-	-	0.001003
L_{PCM} (J kg^{-1})	244000	-	-

3 Results and discussion

3.1 Cooling plate design based on orthogonal experiment

3.1.1 Orthogonal design

The orthogonal experiment integrated with simulations was used with the intention of obtaining the optimum structure of cooling plate, balancing the battery T_{max}, temperature uniformity and ΔP for thermal management based on the PCS. The PCS used in the simulations of the cooling plate design consisted of 80% mass fraction water and 20% mass fraction n-octadecane microcapsules. The design factors including number the of cooling channels, total width of the cooling channels and thickness of the cooling channels can be validated and optimized for heat dissipation. In order to prolong the lifetime of the lithium ion battery and improve the available SOC of the battery system, the battery T_{max} and ΔT_{max} need to be controlled and thus their upper limits were set to 313 K and 5 K, respectively. Meanwhile, lower ΔP of coolant with same mass flow rate resulted in lower energy consumption.

A factorial design was considered with all possible factor level combinations. More efficient designs were received using orthogonal arrays with only a fraction of all possible factor level combinations. Orthogonal arrays were usually denoted by the number of performed experiments and the number of levels per factor and the number of factors.

The cooling plate with channels made of aluminum was set between two adjacent pouch batteries and its length and width were equal to that of the battery. In the upfront simulation and experiment of the pouch battery, it was found that the maximum temperature of the area near the electrode tabs was higher than that farther from the electrode tabs as the heat generation was non-uniform during the 2C discharging process. Consequently, the inlet of the channels was set at the upper end of the cooling plate which is nearest to the electrode area for better cooling performance. In order to decrease the ΔP, the channels were designed to be straight. Channels were uniformly distributed to decrease the temperature difference in the horizontal direction. The structure of the battery module and cooling plate are shown in Fig. 1.

The L16 (4^5) orthogonal array matrix with four levels and three factors was employed to assign the considered factors, including the number of cooling channels (n, factor A), total width of cooling channels (w, factor B), thickness of cooling channels (δ, factor C) and levels, as shown in Table 3. The difference of mass flow rate in each cooling channel was neglected. The mass flow rate of the slurry (the total mass flow rate of slurry in one cooling plate) was 1×10^{-4} kg s^{-1} and the volume fraction of the phase change capsule in the slurry was 20%.

Table 3 Levels and factors of the cooling plate design

Level	Factor		
	n (A)	w (B) / mm	δ (C) / mm
I	6	60	2
II	9	75	2.5

III	12	90	3
IV	15	105	3.5

Sixteen trials were carried out according to the L16 (4^5) matrix to complete the optimization process. Each row of the orthogonal array represented a case with a specific combination of factor levels to be tested. In order to avoid any subjective or personal bias, the case order was randomized. The matrix included three factors and each factor covered four levels as shown in Table 3. After the orthogonal experiments and subsequent data analysis, the optimal structural design of the cooling plate was determined. Finally, the experiment was repeated under the optimal structure to verify the data. The sixteen experiments were carried out and the results are shown in Table 4.

Table 4 Values of T_{max}, ΔT_{max} and ΔP with L16(4^5) matrix (discharge rate: 2C)

Simulation number	Factor			Result		
NO.	A	B	C	T_{max} / K	ΔT_{max} / K	ΔP / Pa
1	6	60	2	310.249	5.423	1.251
2	6	75	2.5	310.039	5.420	0.518
3	6	90	3	309.850	5.471	0.2523
4	6	105	3.5	309.650	5.490	0.138
5	9	60	2.5	310.235	5.311	0.738
6	9	75	2	310.056	5.473	1.034
7	9	90	3.5	309.659	5.528	0.178
8	9	105	3	309.797	5.434	0.225
9	12	60	3	310.155	5.306	0.515
10	12	75	3.5	309.922	5.361	0.259
11	12	90	2	309.866	5.595	0.872
12	12	105	2.5	309.737	5.701	0.394
13	16	60	3.5	310.039	5.351	0.421
14	16	75	3	309.937	5.441	0.4122
15	16	90	2.5	309.815	5.530	0.504
16	16	105	2	309.689	5.629	0.757

In this section, the orthogonal experiment integrated with simulations was used in obtaining the effect of 3 factors on the battery cooling performance and the pressure drop of PCS in heat transfer process.

3.1.2 Screening of the optimal structure

In Table 4, the 4 levels of Factor A appear in the test NO.1 ~ NO.4, NO.5 ~ NO.8, NO.9 ~ NO.12, NO.13 ~ NO.16, respectively. The value of T_{max} in the 16 tests were numbered as N_1 ~ N_{16}, respectively. k_i is used to evaluate the effect of each level on the T_{max}. And R is used to evaluate the effect of each factor on the T_{max}. They can be described as Eq. (19) and Eq. (20):

$$\begin{cases} k_1 = (N_1 + N_2 + N_3 + N_4)/4 \\ k_2 = (N_5 + N_6 + N_7 + N_8)/4 \\ k_3 = (N_9 + N_{10} + N_{11} + N_{12})/4 \\ k_4 = (N_{13} + N_{14} + N_{15} + N_{16})/4 \end{cases} \tag{19}$$

$$R = \max(k_1, k_2, k_3, k_4) - \min(k_1, k_2, k_3, k_4) \tag{20}$$

A larger R means a greater influence from the factor. The k_i and R for each factor at different levels are shown in Table 5 and the value of k_i for T_{max}, ΔT_{max} and ΔP are shown in Fig. 3.

Table 5 Range analysis data of simulation

Parameter	T_{max} / K			ΔT_{max} / K			ΔP / Pa		
	A	B	C	A	B	C	A	B	C
k_1	309.947	310.170	309.965	5.451	5.348	5.530	0.540	0.731	0.979
k_2	309.937	309.989	309.956	5.436	5.424	5.490	0.544	0.556	0.538
k_3	309.920	309.797	309.935	5.491	5.531	5.413	0.510	0.452	0.351
k_4	309.870	309.718	309.818	5.488	5.563	5.432	0.524	0.379	0.249
R	0.077	0.452	0.147	0.055	0.215	0.117	0.034	0.352	0.730

The results in Fig. 3(a) show that the T_{max} decreased as the Factor A, B, C increased. The increasing Factor A, B, C lead to lower velocity of coolant. As a result, the heat transfer process between battery and PCS is prolonged and more heat is removed by the coolant. As the factor with

a larger R_i has a bigger influence on the relevant evaluation index [27], the effect of factors on the battery T_{max} are listed as follows: factor B (w) > factor C (δ) > factor A (n). This is reflected in Fig. 3(a).The combination of n = 15 (T_{max} = 309.870 K), w = 105mm (T_{max} = 309.718 K) and δ = 3.5 mm (T_{max} = 309.818 K) gave the lowest value of k_{ij} for each factor. As a result, the optimum structure is $A_4B_4C_4$. As Fig. 3(b) shows, the T_{max} increased as the Factor B increased. But the effect of the3 Factors on the battery ΔT_{max} is small and it indicates that it is the non-uniform heat generation playing a vital role in the battery ΔT_{max}. n = 9 and δ = 3 mm gave the lowest value of k_{ij} for Factor A and Factor C. When the evaluation index is ΔT_{max}, the optimum structure is $A_2B_1C_3$. Fig. 3(c) shows that the ΔP decreased with the increasing Factor B and C. It results from the velocity of coolant decreases with the increasing Factor B and C. Similarly, the optimum structure should be $A_3B_4C_4$ to decrease the energy consumption.

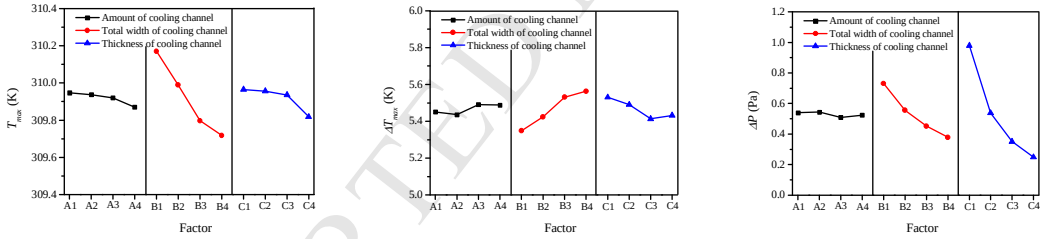

(a) (b) (c)

Fig. 3 Mean values of each factor for T_{max} (a), ΔT_{max} (b) and ΔP (c)

As discussed before, the optimization programs for T_{max}, ΔT_{max} and ΔP were $A_4B_4C_4$, $A_2B_1C_3$ and $A_3B_4C_4$, respectively. These tree programs were also simulated with Fluent and the results are shown in Table 5. As shown in Fig. 3, it is obvious that the influence of the number of cooling channels on the T_{max}, ΔT_{max} and ΔP was small. As the total width of the cooling channel increased, the T_{max} showed opposite trend in comparison to ΔT_{max} and ΔP. The T_{max}, ΔT_{max} and ΔP decreased with increasing channel thickness. Thus it was impossible to minimize the T_{max}, ΔT_{max} and ΔP in

the same program, as shown in Table 6. It was necessary to find the program which could keep a balance in the values of T_{max}, ΔT_{max} and ΔP. In Table 4, the T_{max} and ΔP of program $A_1B_4C_4$ (No.4 in Table 4) was smallest and the ΔT_{max} was 0.18 K higher than that of the smallest value obtained amongst the programs. As the variation of ΔT_{max} was smaller than T_{max} and ΔP, among the 16 programs in Table 4 the $A_1B_4C_4$ could be the optimization program in keeping balance of T_{max}, ΔT_{max} and ΔP.

Table 6 Single experiment index optimization program

Evaluation index	Optimization program	Significance of each factor	Result		
			T_{max} / K	ΔT_{max} / K	ΔP / Pa
T_{max}	$A_4B_4C_4$	B>C>A	309.571	5.510	0.169
ΔT_{max}	$A_2B_1C_3$	B>C>A	311.205	5.152	0.306
ΔP	$A_3B_4C_4$	C>B>A	309.597	5.503	0.121

The difference between No.4 ($A_1B_4C_4$) and $A_4B_4C_4$ was the number of the cooling channels. As the channel number has only a slight influence on the cooling performance, the temperature field and energy consumption of the two were similar. $A_1B_4C_4$ was better than $A_4B_4C_4$. Similarly, the $A_1B_4C_4$ was better than $A_4B_4C_4$. Compared with $A_1B_4C_4$, the ΔT_{max} of $A_2B_1C_3$ was 0.338 K lower but the T_{max} of $A_2B_1C_3$ was 1.56 K higher. This is because the increasing channel width heavily influenced the ΔT_{max}. As a result, considering the balance of T_{max}, ΔT_{max} and ΔP and practical use, the $A_1B_4C_4$ was selected as the optimal structure. Thus the optimal level for each factor was determined as follows: 6 cooling channels, 105 mm total width of cooling channels with a thickness of 3.5 mm. Fig. 4 shows the temperature field cloud image of the battery center section with cooling and without cooling after 2C discharging.

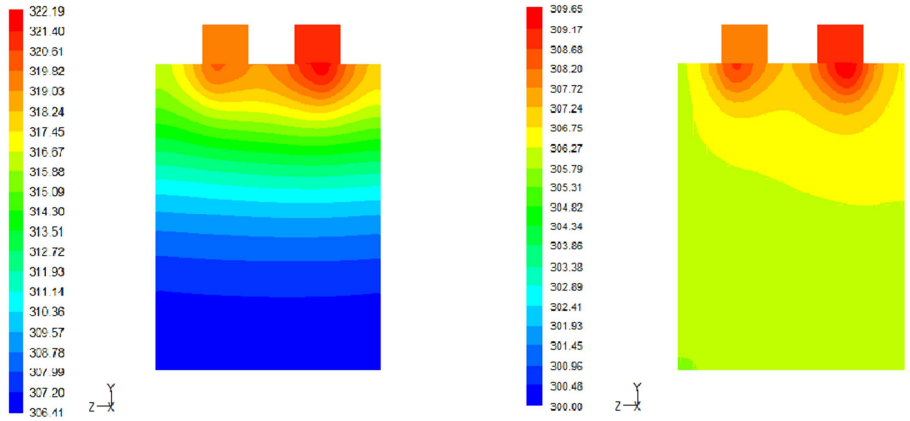

(a) (b)

Fig. 4 Temperature field cloud image of battery center section without cooling (a) and with PCS cooling (b) after 2C discharging

In this section, the optimum structure of the cooling plate with 6 mini channels, whose total width was 105 mm and thickness was 3.5 mm was obtained with orthogonal experiment and simulations. And this cooling plate can balance the battery cooling performance and the energy consumption of PCS.

3.2 The comparison of PCS with other liquids in cooling performance

In order to compare the cooling performance of the PCS with other liquids, the cooling plate with the PCS (80 % mass fraction water and 20 % mass fraction n-octadecane microcapsule), pure water, glycol solution (50% mass fraction water and 50% mass fraction glycol) and mineral oil were utilized to cool the 2C discharging battery, respectively. The material properties of the different liquid coolants are shown in Table 7. The T_{max} and ΔT_{max} plots of the battery with different coolants versus the mass flow rate are shown in Fig. 5.

Table 7 Material properties of different liquid coolant [15][20]

Item	PCS (20 microcapsule / 80 water)	Water	Glycol solution (50 water / 50 glycol)	Mineral oil
ρ (kg m^{-3})	960	998.2	1069	924.1
c_p (J kg^{-1} K^{-1})	-	4182	3323	1900

λ (W m^{-1} K^{-1})	0.4342	0.6	0.3892	0.13
υ (kg m^{-1} s^{-1})	0.001935	0.001003	0.002758	0.005175

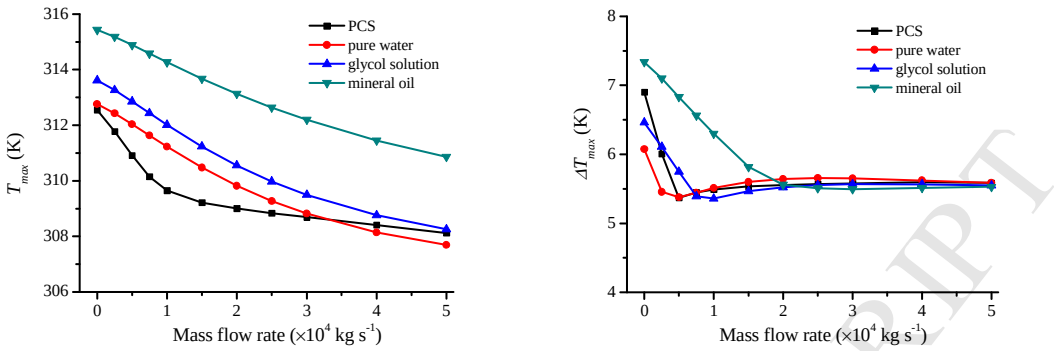

(a) (b)

Fig. 5 T_{max} plot (a) and ΔT_{max} plot (b) of battery cooled by different liquid coolant versus mass flow rate

The T_{max} plot of battery shows that after 2 C discharging the battery T_{max} decreased with increasing mass flow rate of coolant. The T_{max} plot of battery cooled by pure water, glycol solution and mineral oil shows a similar trend. Compared with glycol solution and mineral oil with the same mass flow rate, pure water performed best in heat dissipation. Profiting from high λ, the heat transfer in the pure water was faster coupled with a smaller temperature rise resulting from the high c_p. As a result, during the heat convection, the enlarged average temperature difference between the battery and pure water improved the heat dissipation. In comparison, the small λ and c_p of the mineral oil led to a high temperature rise. On the other hand, with the increasing mass flow rate, the T_{max} plot of the battery cooled by the PCS showed a different trend. When the mass flow rate is less than 1×10^{-4} kg s^{-1}, after 2 C discharging, the T_{max} of the battery decreases with an increase in the mass flow rate. However, further increase in the mass flow rate results in a decline in this trend. Interestingly, when the mass flow rate was higher than 3.5×10^{-4} kg s^{-1}, the T_{max} of the battery cooled by the PCS was higher than that of the battery cooled by pure water. In the heat convection process, the temperature of the PCS was consistently lower than the phase change temperature of the core in the microcapsule, when the mass flow rate exceeded 3.5×10^{-4} kg s^{-1}. In

this temperature range, the c_p and λ of the PCS was lower than that of pure water. Both the lower parameters led to a small average temperature difference and poor cooling performance. When the mass flow rate was 1×10^{-4} kg s^{-1}, the difference between the T_{max} of the battery cooled by PCS and that by pure water was maximized. In this case, the advantage of the PCS on the cooling performance was the most significant. A similar conclusion was also obtained by Rao in his research on flow characteristics of microencapsulated phase change material suspensions flowing through rectangular mini channels[44]. Therefore, when using a PCS as coolant, the optimal mass flow rate of the PCS of different concentrations should be determined to achieve the optimal cooling effect.

The ΔT_{max} plots of the battery cooled by the different liquid coolants showed similar trends. As the mass flow rate increased, the battery ΔT_{max} decreased rapidly to a stable value. When the liquid coolant remained stationary, the ΔT_{max} of battery cooled by the pure water and glycol solution was lower than that of the battery cooled by the PCS. This is because the λ was the key factor during the heat conduction process. When the liquid coolant flowed, the ΔT_{max} of the battery cooled by the PCS decreased rapidly. When the mass flow rate exceeded 1×10^{-4} kg s^{-1}, the difference of battery ΔT_{max} cooled by PCS, pure water and glycol solution was less than 0.2 K. The ΔT_{max} of the battery cooled by mineral oil declined slowly at a constant rate. It remained at 5.5 K when the mass flow rate was higher than 2×10^{-4} kg s^{-1}. There was no significant advantage for the PCS cooling in decreasing the battery ΔT_{max}. The non-uniformity of the battery heat generation and low λ_{bat} were the key factors resulting in the non-uniformity of the temperature field.

In the channels, the ΔP was related to the mass flow rate and viscosity. From the Fig. 6, it is observed that the ΔP variation of the different liquid coolants has a linear relationship with the

mass flow rate. When the mass flow rate was 1×10^{-4} kg s^{-1}, the ΔP of the PCS was less than that of pure water flowing at 2×10^{-4} kg s^{-1}. Furthermore, the cooling performance of the PCS was better than that of pure water, as shown in Fig. 5. In this case, compared with the pure water, the PCS had a better cooling performance and lower energy consumption.

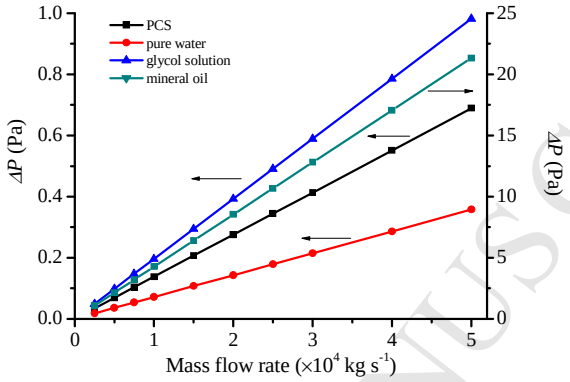

Fig. 6 ΔP of different liquid coolant in the channels versus mass flow rate

In this section, battery cooling performance of the PCS, pure water, glycol solution and mineral oil were compared. The effect of these 4 coolants on battery ΔT_{max} was approximate when the mass flow rate exceeded 2×10^{-4} kg s^{-1}. Compared with other coolants, the PCS showed the superiority in restraining the battery T_{max}. And the ΔP of the PCS in the mini channel cooling plate is higher than that of pure water but lower than that of glycol solution and mineral oil.

3.3 Effects of mPCM's phase change temperature

The phase change temperature of PCMs used in the battery thermal management influenced the battery temperature field. In order to investigate the effect of phase change temperature of microcapsule in the PCS on the cooling performance, the melting point of the core material in the microcapsule was changed in the simulation. The simulation results of the battery temperature are shown in Fig. 7.

As the melting point of the core material in the microcapsule increased, the battery T_{max} after 2 C discharging increased continuously. Nevertheless, the ΔT_{max} of battery changed slightly. When the temperature of the mPCM during the heat convection process was lower than the melting point, the c_p of the PCS was small and the temperature rising of PCS was significant. It led to a decrease in the average temperature difference of battery and PCS. As a result, the heat dissipation of the PCS declined. If the temperature of the mPCM exceeded the melting point, the phase change process of the PCM was activated and it started to absorb heat. In the discharging process, the T_{max} and T_{min} of the battery increased synchronously and the ΔT_{max} of the battery was almost unchanged. However, it would be inappropriate to lower the melting point too much. If the environment temperature exceeded the melting point of the core and the PCS could not be cooled by another cold source, the microcapsule might melt before cooling the module. As a result, the PCS will lose the ability to absorb more heat in the form of the phase change enthalpy of the microcapsule. In other words, if the temperature of the PCS could be cooled lower than the melting point, the lower phase change temperature of the core in the microcapsules contributes to restraining the battery ΔT_{max}. Therefore, in battery thermal management based on PCS, the selection of the microcapsule melting point should depend on the operating environment and the conditions of the cooling system to involve the latent heat[45].

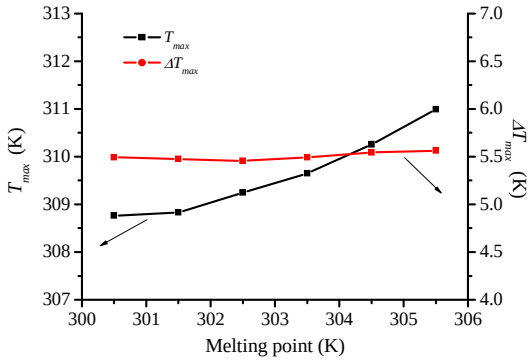

Fig. 7 Battery T_{max} and ΔT_{max} cooled by PCS versus melting point of mPCM

In this section, the effect of mPCM's melting point on battery cooling was investigated. The results show that battery T_{max} rises with the increasing melting point but the battery ΔT_{max} is almost unchanged.

3.4 Effects of PCS's mass flow rate and concentration

The PCS's mass flow rate and concentration are the important factors that influence the cooling performance of battery thermal management based on the PCS. In order to find the combined effect of these two key factors on the cooling performance, the temperature field of the battery cooled by different concentrations at different mass flow rate was simulated. The results are shown in Fig. 8.

As shown in Fig. 8(a), the T_{max} curve of the battery cooled by a PCS with a low concentration was close to that of the battery cooled by pure water, due to the similar λ and c_p. Raising the PCS's concentration made a contribution to the increasing equivalent c_p of the PCS within the phase change temperature range of the mPCM . Fig. 8(b) shows the ΔT_{max} of the battery cooled by different concentrations of the PCS versus the mass flow rate. As the mass flow rate of the PCS increased, the ΔT_{max} of the battery decreased rapidly then increased slightly and remained stable. When the mass flow rate was 0.5×10^{-4} kg s^{-1}, the ΔT_{max} of the battery cooled by different concentrations of the PCS and pure water was the same and at the minimum value. The difference of ΔT_{max} was no more than 0.3 K. The value of ΔT_{max} was always higher than 5K, even though both the concentration and the mass flow rate of PCS increased.

The T_{max} curves for concentrations over 15% seemed dense, while the curves for concentration

lower than 10% were scattered, meaning that the enhancement of the cooling performance by raising the concentration was limited. The T_{max} of the battery cooled by different concentrations of PCS declined with increasing mass flow rate and this declining trend diminished gradually. The higher the concentration, the more obvious the decline in the trend. The reason being that the increasing c_p led to a lower temperature of the PCS and a larger average temperature difference during the heat transfer process. When the mass flow rate was low, the T_{max} of the battery was strongly affected. When the mass flow rate was less than 0.25×10^{-4} kg s^{-1}, the PCS temperature was higher than the melting point of mPCM. The cooling performance was improved with the increasing equivalent c_p caused by higher concentration. As the mass flow rate increased, the difference of T_{max} of the battery cooled by different concentrations of PCS expanded gradually. When the flow rate was 1×10^{-4} kg s^{-1}, the difference was greatest. At that stage, the phase change latent heat of mPCM played a dominant role. As the mass flow rate increased from 1×10^{-4} kg s^{-1} to 2×10^{-4} kg s^{-1}, the difference in cooling performance decreased gradually. As the mass flow rate increased to a specific value, the cooling performance of the PCS was equal to that of pure water. The value was different with the PCS's concentration. If the mass flow rate exceeded the value, the PCS's cooling performance was worse than that of pure water. The reason was that the temperature of the PCS was always lower than the melting point of the mPCM during the heat transfer process but the λ and c_p of the PCS was lower than that of pure water. When the flow rate was higher than 4×10^{-4} kg s^{-1}, the cooling performance decreased with increasing PCS concentration as the λ and c_p decreased. At that stage, the λ and c_p played dominant role.

The Fig. 8(c) shows the difference between T_{max} of the battery cooled by the PCS and pure water versus the mass flow rate. The cooling performance of different concentrations of PCS with

different mass flow rates was compared with that of pure water. In each curve of different concentrations of the PCS, there were two points that were worthy of attention. One point indicated that the difference between T_{max} of the battery cooled by the PCS and pure water was largest. The corresponding mass flow rate of this point was identified as the optimal value. And the other point, whose corresponding mass flow rate was identified as the critical value, donated the equal T_{max} of the battery cooled by the PCS and pure water. When the mass flow rate was higher than the critical value, the PCS's cooling performance was worse than that of pure water. By interpolation on Fig.8(c) the optimal value and the critical value of the mass flow rate for different concentrations of the PCS were determined. As shown in Fig. 8(d), both the optimal value and the critical value of the mass flow rate decreased with the rising concentration. This results from the increasing c_p of the PCS in the phase change temperature range caused by the increasing concentration. For different concentrations of the PCS used in the battery thermal management, to maximize the cooling performance, the corresponding point of PCS's mass flow rate should be close to the black line (the optimal value) in Fig. 8(d). To avoid worsening the cooling performance, the corresponding point should be lower than the red line (the critical value) in Fig. 8(d).

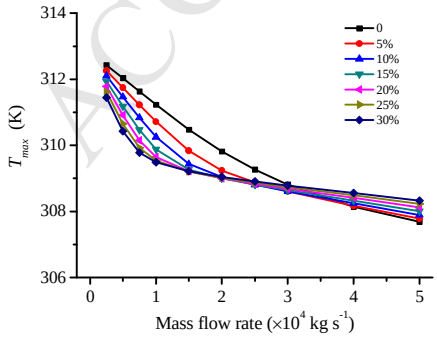

(a)

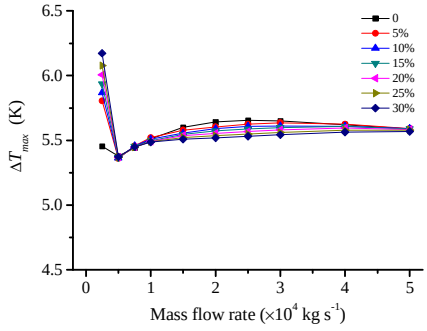

(b)

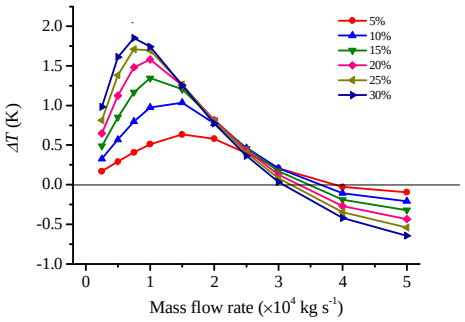

(c)

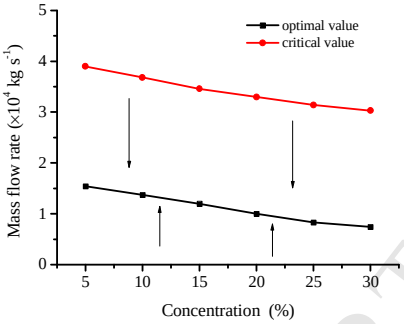

(d)

Fig. 8 T_{max} plot (a) , ΔT_{max} plot (b) of battery cooled by different concentration PCS versus mass flow rate; difference between T_{max} of battery cooled by PCS and pure water versus mass flow rate (c); the optimal value and the critical value of mass flow rate for different concentration PCS (d)

To investigate the energy consumption variation in PCS cooling battery module, the ΔP of different concentrations of the PCS and pure water in the cooling channels with increasing mass flow rate were simulated. The simulation results are shown in Fig. 9(a).

It showed that the ΔP of the PCS and pure water in the cooling channels increased linearly with the rising mass flow rate, resulting from the straight cooling channels and the low mass flow rate. Keeping the mass flow rate unchanged, the ΔP of the PCS increased with concentration, as the viscosity was improved. The higher the concentration, the larger the increasing rate of ΔP. When considering the mass flow rate of liquid coolant alone, the PCS cooling seemingly had no advantage in energy consumption, compared with pure water.

Nevertheless, cooling performance should be considered to survey whether the PCS cooling had the edge over the pure water in energy consumption. The mass flow rate of the different concentrations of PCS and pure water were compared, under the conditions that the battery T_{max} be restrained to the same temperature after 2C discharging. Fig. 8(a) was magnified and some auxiliary lines added to draw Fig. 9(b). Firstly, the interpolation method was used to get the mass flow rate and ΔP under the circumstance of the battery T_{max} being restrained to 310 K. The results

are shown in Fig. 9(c). And it showed that with the increase in concentration the mass flow rate decreased and the ΔP decreased then increased. When the concentration of the PCS was 15% the energy consumption was lowest. Additionally, the ΔP of the different concentrations of the PCS was always higher than that of pure water. It revealed that the PCS cooling had advantage in energy consumption over pure water, as the cooling target for battery T_{max} was 310 K. Then the cooling target was set to 311 K, 309 K and 308.5 K, respectively. The ΔP of the different concentrations of the PCS and pure water was determined using the previous method. The results are displayed in Fig. 9(d). As shown, when the cooling target was 310 K and 311 K, the ΔP of the PCS was lower than that of pure water. The PCS cooling had the advantage in energy consumption. When the cooling target was 309 K, the ΔP of PCS, with a concentration less than 12%, was lower than that of pure water. When the cooling target was 308.5 K, the energy consumption of the PCS cooling was higher than that of pure water. The reason being that the phase change enthalpy in the mPCM was not completely utilized as the PCS's concentration increased. However, as the cooling performance was improved slightly, the viscosity rose significantly. Yet as discussed before, the PCS cooling had the advantage in energy consumption compared with water cooling, when the cooling target for the battery T_{max} was higher than 309 K and the concentration of the PCS was appropriate.

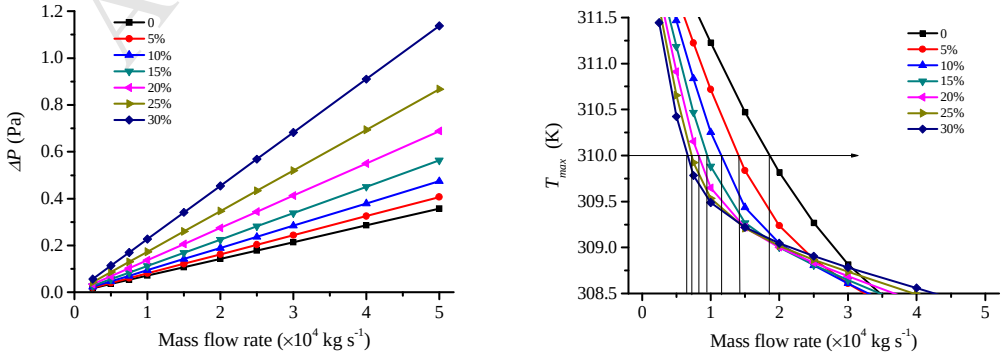

(a) (b)

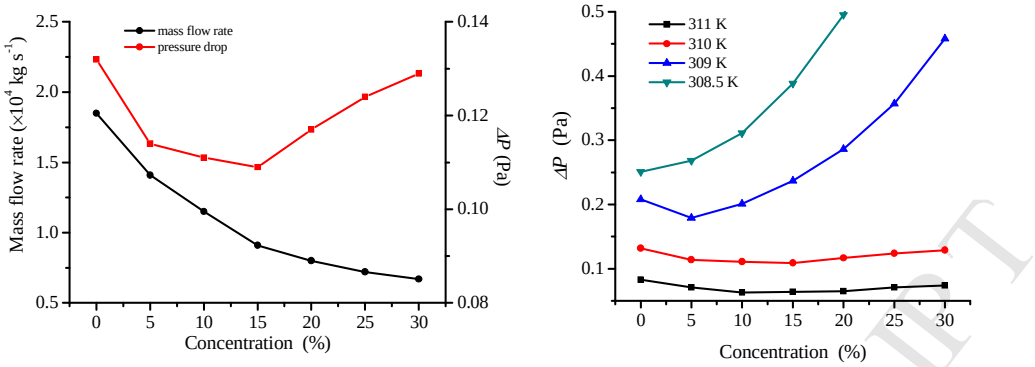

(c) (d)

Fig.9 ΔP plot (a), T_{max} plot (b) of different concentration PCS versus mass flow rate; ΔP and mass flow rate of different concentration PCS under the circumstance of the battery T_{max} being restrained to 310 K (c); ΔP of different concentration PCS with different cooling target for battery T_{max} (d)

In this section, the effect of PCS's mass flow rate and concentration battery cooling was investigated. When the mass flow rate exceeded the critical value, the cooling performance of the PCS was worse than that of pure water. When the cooling target for the battery $T_{\max}$ was higher than 309 K, at an appropriate concentration, the PCS cooling had the advantage in energy consumption compared with water cooling.

3.5 Dimensionless empirical formula

In this section, the average h of different concentrations of PCS versus mass flow rate was calculated to further indicate the effect of the PCS's physical parameters and the flow on the heat dissipating process. The results are shown in Fig.10.

With increasing h, the cooling performance was enhanced and the T_{max} of battery module declined. As a result, the variation of h in Fig.10 and variation of T_{max} in Fig. 8(a) were correlated. In the cooling pate with PCS or pure water, the h increased with the increasing mass flow rate. Compared with that of pure water as the coolant, the curve of h in the PCS cooling showed a different variation trend. The h in water cooling increased with a relative constant rate with

increasing mass flow rate, resulting from the unchanged c_p. When the mass flow rate was high, the rising trend of h in the different concentration PCS cooling declined gradually. The higher the concentration of mPCM was, the more obvious the variation trend would be. What's more, as the mass flow rate exceeded a certain value, the h of the PCS cooling was less that of the pure water cooling. The higher the concentration of mPCM, the lower the value. It indicated that there was a limit in the contribution of mass flow rate and concentration to h in PCS cooling. Wang[46] made similar conclusions in their work. It showed that, the gain of the cooling system reduces strongly after a certain threshold of liquid flow rate.

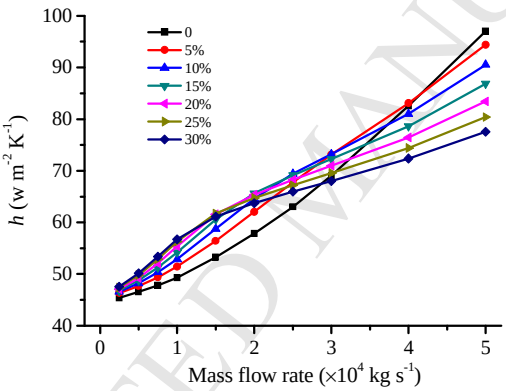

Fig. 10 The average h of different concentration PCS versus mass flow rate

In order to intuitively describe the simulation results of battery thermal management based on PCS, the heat transfer effect of the cooling plate was dealt with a dimensionless method and Fig. 10 was converted to Fig. 11. The *Pr* represents the physical characteristics of the PCS with different concentrations of mPCM. As the mPCM concentration was 0 %, 5 %, 10 %, 15 %, 20 %, 25 % and 30 %, the value of *Pr* changed from 7 to 29.2. The *Re* represents the flow characteristics of the PCS in the cooling plate. The value of *Re* increased with the increasing mass flow rate of PCS. As the velocity of the PCS in the cooling channel was small, the *Re* was less than 10. The *Nu* represents the performance in the convective heat transfer process. The relation of *Nu*, *Re* and *Pr*

can be expressed as[47]:

$$Nu = CRe^{m}Pr^{n} \tag{21}$$

By taking the logarithm of *Nu*, *Re* and *Pr*, a new form of the equation was obtained:

$$\ln Nu = C + m\ln Re + n\ln Pr \tag{22}$$

With multiple linear regression, the date in Fig.11 can be expressed with the empirical formula in dimensionless form, as Eq. (22) shows. It was used to predict the effect of the PCS's physical parameters and flow characteristics on the heat transfer performance.

$$Nu = 0.1829Re^{0.2103}Pr^{0.5344} \tag{23}$$

where the R^2 of the empirical formula was 0.9249.

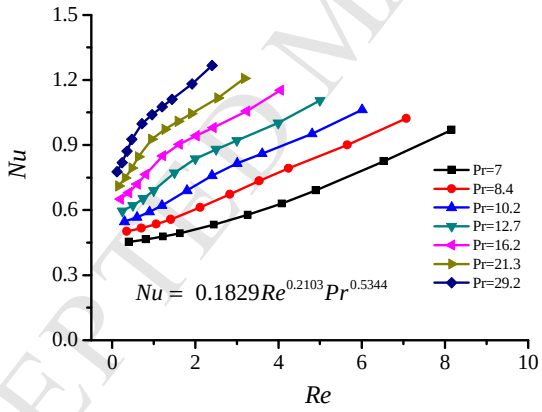

Fig. 11 The dimensionless number about *Nu-Re-Pr*

In Fig. 11, the exponentiation of *Re* and *Pr* in the dimensionless empirical formula was higher than 0. It indicates that both the mass flow rate and concentration of the PCS contributed to the increasing convective heat transfer. As shown in Fig. 11, in the region made up of 80 points, for a constant value of *Re*, the *Nu* increased with the increasing *Pr*. It indicates that the increasing *h* results from increasing PCS's concentration. Keeping the *Pr* unchanged, the *Nu* increased with the increasing *Re*. When the *Pr* was higher than 10, there was an inflection point in the curve. As

the *Pr* increased, the corresponding *Re* of the inflection points decreased. To the left of the inflection point, *Nu* increased with *Re* in a high rising rate. To the right side of the inflection point, the rising rate decreased. The occurrence of inflection points indicates that the effect of mass flow rate on the cooling performance was weakened.

Similarly, the dimensionless empirical formula can be used describing the effect of the PCS's physical parameters and flow characteristic on the restraining of T_{max} in the cooling process. As the maximum excess temperature (θ_{max}) was used to describe the difference of the T_{max} and T_0, the excess temperature dimensional number Θ can be used to show the cooling performance, as in Eq. (24):

$$\Theta = \frac{\theta_{\max}}{\theta_{\max 0}} = \frac{T_{\max} - T_0}{T_{\max 0} - T_0} \tag{24}$$

where the T_{max0} was the maximum temperature of battery without cooling after the 2 C discharge process. The better the cooling performance was, the smaller the Θ was, as the Θ decreased with decreasing T_{max}.

Fig. 8(a) was converted to Fig. 12 and the empirical formula with dimensionless form was obtained, as Eq. (25) shows.

$$\Theta = 0.7058 Re^{0.8733} Pr^{0.8526} \tag{25}$$

where the R^2 of the empirical formula was 0.9336.

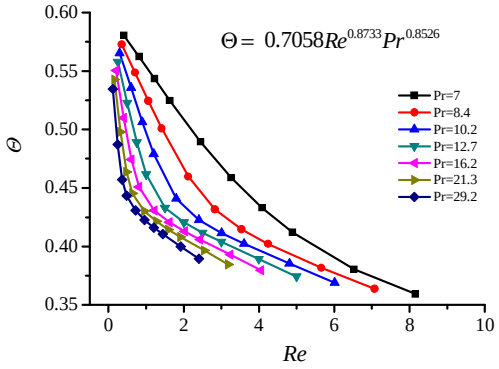

Fig. 12 The dimensionless number about *Θ-Re-Pr*

In this section, the effect of PCS's physical parameters and flow characteristics on the *h* and T_{max} were expressed with correlations relevant to the *Re* and *Pr*. The correlations can be used forecasting the simulation results which were not calculated in this paper, such as different concentration and mass flow rate. And the correlations can offer the reference for the arrangement of experimental scheme and the engineering application.

4 Conclusions

This paper presented work on battery thermal management based on the phase change slurry and mini channel cooling plate. The optimum structure of the cooling plate was designed with the orthogonal matrix experimental method. The cooling performance of the PCS and that of other liquid coolants was compared. The effect of the mPCM's phase change temperature, the PCS's mass flow rate and concentration on the cooling performance and energy consumption was investigated. Lastly, a dimensionless empirical formula was obtained to predict the effect of the PCS's physical parameters and flow characteristics on the heat transfer and cooling performance. The main results include:

(1) The optimum structure of the cooling plate with 6 mini channels, whose total width was 105 mm and thickness was 3.5 mm, could balance the cooling performance with energy

consumption.

(2) The cooling performance of the PCS consisting of 20% n-octadecane microcapsules and 80% water was better than that of pure water, glycol solution and mineral oil, when the mass flow rate was less than 3×10^{-4} kg s^{-1}. As the phase change temperature of microcapsules increased from 300.5 K to 305.5 K, the T_{max} of battery cooled by PCS increased and the ΔT_{max} changed slightly.

(3) When the mass flow rate exceeded the critical value, the cooling performance of the PCS was worse than that of pure water. When the cooling target for the battery T_{max} was higher than 309 K, at an appropriate concentration, the PCS cooling had the advantage in energy consumption compared with water cooling.

(4) Both an increase in mass flow rate and concentration of the PCS led to a higher convective heat transfer coefficient. The effect of physical parameters and flow characteristics of the PCS on the h and T_{max} were expressed with flowing formulas: $Nu = 0.1829Re^{0.2103}Pr^{0.5344}$ and $\Theta = 0.7058Re^{0.8733}Pr^{0.8526}$, respectively.

Acknowledge

The authors would like to express their gratitude for the support of the National Natural Science Foundation of China: No.51477171, No.51607176 and No.51806223; and the Royal Society (IE150598).

References

[1] Ye YH, Shi YX, Saw LH, Tay AAO. Simulation and evaluation of capacity recovery methods for spiral-wound

lithium ion batteries. J Power Sources 2013; 243: 779-789.

[2] Bandhauer T, Garimella S, Fuller TF. Electrochemical-Thermal Modeling to Evaluate Battery Thermal Management Strategies II. Edge and Internal Cooling. J Electrochem Soc 2015; 162: A125-A136.

[3] Saw LH, Ye Y, Tay AAO. Feasibility study of Boron Nitride coating on Lithium-ion battery casing. Appl Therm Eng 2014; 73: 154-161.

[4] An ZJ, Jia L, Ding Y, Dang C, Li XJ. A Review on Lithium-ion Power Battery Thermal Management Technologies and Thermal Safety. J Therm Sci 2017; 26: 391–412.

[5] Liang JL, Gan YH, Li Y. Investigation on the thermal performance of a battery thermal management system using heat pipe under different ambient temperatures. Energ Convers Manage 2018; 155: 1–9.

[6] An ZJ, Jia L, Li XJ, Ding Y. Experimental investigation on lithium-ion battery thermal management based on flow boiling in mini-channel. Appl Therm Eng 2017; 117: 534-543.

[7] Al-Zareer M, Dincer I, Rosen MA. Development and evaluation of a new ammonia boiling based battery thermal management system, Electrochim Acta 2018; 280: 340-352.

[8] Bai FF, Chen MB, Song WJ, Feng ZP, Li YL, Ding YL. Thermal management performances of PCM/water cooling-plate using for lithium-ion battery module based on non-uniform internal heat source. Appl Therm Eng 2017; 126:17–27.

[9] Ling ZY, Zhang ZG, Shi GQ, Fang XM, Wang L, Gao XN, Fang YT, Xua T, Wang SF, Liu XH. Review on thermal management systems using phase change materials for electronic components, Li-ion batteries and photovoltaic modules. Renew Sust Energ Rev 2014; 31: 427–438.

[10] Malik M, Dincer I, Rosen MA. Review on use of phase change materials in battery thermal management for electric and hybrid electric vehicles. Int J Energ Res 2016; 40: 1011–1031.

[11] Javani N, Dincer I, Naterer GF, Rohrauer GL. Modeling of passive thermal management for electric vehicle battery packs with PCM between cells. Appl Therm Eng 2014; 73: 307–316.

[12] Mettawee EBS, Assassa GMR. Thermal conductivity enhancement in a latent heat storage system. Sol Energ 2007; 81: 839–845.

[13] Wu WX, Wu W, Wang SF. Thermal optimization of composite PCM based large-format lithium-ion battery modules under extreme operating conditions. Energ Convers Manage 2017; 153: 22–33.

[14] Libeer W, Ramos F, Newton C, Alipanahrostami M, Depcik C, Li XL. Two-phase heat and mass transfer of

phase change materials in thermal management systems. Int J Heat Mass Tran 2016; 100: 215–223.

[15] Wang ZW, Zhang HY, Xia X. Experimental investigation on the thermal behavior of cylindrical battery with composite paraffin and fin structure. Int J Heat Mass Tran 2017; 109: 958–970.

[16] Shi S, Xie YQ, Li M, Yuan YP, Yu JZ, Wu HW, Liu B, Liu N. Non-steady experimental investigation on an integrated thermal management system for power battery with phase change materials. Energ Convers Manage 2017; 138: 84–96.

[17] Liu R, Chen JX, Xun JZ, Jiao K, Du Q. Numerical investigation of thermal behaviors in lithium-ion battery stack discharge. Appl Energ 2014; 132: 288–297.

[18] Chen DF, Jiang JC, Kim GH, Yang CB, Pesaran A. Comparison of different cooling methods for lithium ion battery cells. Appl Therm Eng 2016; 94: 846–854.

[19] Jin LW, Lee PS, Kong XS, Fan Y, Chou SK. Ultra-thin mini-channel LCP for EV battery thermal management. Appl Energ 2014; 113: 1786–1794.

[20] Rao ZH, Qian Z, Kuang Y, Li YM. Thermal performance of liquid cooling based thermal management system for cylindrical lithium-ion battery module with variable contact surface. Appl Therm Eng 2017; 123: 1514–1522.

[21] Zhao JT, Rao ZH, Li YM. Thermal performance of mini-channel liquid cooled cylinder based battery thermal management for cylindrical lithium-ion power battery. Energ Convers Manage 2015; 103: 157–165.

[22] Panchal S, Khasow R, Dincer I, Agelin-Chaab M, Fraser R, Fowle M. Thermal design and simulation of mini-channel cold plate for water cooled large sized prismatic Lithium-ion battery. Appl Therm Eng 2017; 122: 80–90.

[23] Panchal S, Dincer I, Agelin-Chaab M, Fraser R, Fowle M. Experimental and theoretical investigations of heat generation rates for a water cooled LiFePO4 battery. Int J Heat Mass Trans 2016; 101: 1093–1102.

[24] Yu QH, Tchuenbou-Magaia F, Al-Duri B, Zhang ZH, Ding YL, Li YL. Thermo-mechanical analysis of microcapsules containing phase change materials for cold storage. Appl Energ 2018; 211: 1190-1202.

[25] Chen BJ, Wang X, Zeng RL, Zhang YP, Wang XC, Niu JL, Li Y, Di HF. An experimental study of convective heat transfer with microencapsulated phase change material suspension: laminar flow in a circular tube under constant heat flux. Exp Therm Fluid Sci 2008; 32: 1638–1646.

[26] Wang XC, Niu JL, Li Y, Zhang YP, Wang X, Chen BJ, Zeng RL, Song QW. Heat transfer of microencapsulated PCM slurry flow in a circular tube. AIChE J. 2008; 54: 1110–1120.

[27] Delgado M, Lázaro A, Mazo J, Marín JM, Zalba B. Experimental analysis of a microencapsulated PCM slurry as thermal storage system and as heat transfer fluid in laminar flow. Appl Therm Eng 2012; 36: 370–377.

[28] Griffiths PW, Eames PC. Performance of chilled ceiling panels using phase change material slurries as the heat transport medium. Appl Therm Eng 2007; 27: 1756–1760.

[29] Lin KP, Zhang YP, Xu X, Di HF, Yang R, Qin PH. Experimental study of under-floor electric heating system with shape-stabilized PCM plates. Energ Buildings 2005; 37: 215–220.

[30] Entrop AG, Brouwers HJH, Reinders AHME. Experimental research on the use of micro-encapsulated phase change materials to store solar energy in concrete floors and to save energy in Dutch houses. Sol Energ 2011; 85: 1007–1020.

[31] Hao YL, Tao YX, A numerical model for phase-change suspension flow in microchannels. Numer Heat Transf A-Appl 2004; 46: 55–77.

[32] Zhang YL, Wang SF, Rao ZH, Xie JF. Experiment on heat storage characteristic of microencapsulated phase change material slurry. Sol Energ Mat Sol C 2011; 95: 2726–2733.

[33] Roberts NS, Refat A, Kurdi J, Al-Muhtaseb SA, Farid MM. Efficacy of using slurry of metal-coated microencapsulated PCM for cooling in a micro-channel heat exchanger. Appl Therm Eng 2017; 122: 11–18.

[34] Zhang XW, Kong X, Li GJ, Li J. Thermodynamic assessment of active cooling/heating methods for lithium-ion batteries of electric vehicles in extreme conditions. Sol Energ 2014; 64: 1092-1101.

[35] Chen MB, Bai FF, Song WJ, Lv J, Lin SL, Feng ZP, Li YL, Ding YL. A multilayer electro-thermal model of pouch battery during normal discharge and internal short circuit process. Appl Therm Eng 2017; 120: 506–516.

[36] Roy SK, Avanic BL. Turbulent heat transfer with phase change material suspensions. Int J Heat Mass Transf 2001; 44: 2277–2285.

[37] Chen L, Wang T, Zhao Y, Zhang XR. Characterization of thermal and hydrodynamic properties for microencapsulated phase change slurry (MPCS). Energ Convers Manage 2014; 79: 317-333.

[38] Zhang P, Ma ZW, Wang RZ. An overview of phase change material slurries: MPCS and CHS. Renew Sustain Energ Rev 2010; 14: 598–614.

[39] Charunyaorn P, Sengupta S, Roy SK. Forced convection heat transfer in microencapsulated phase change material slurries: flow in circular ducts. Int J Heat Mass Transf 1991; 34: 819–833.

[40] Mulligan JC, Colvin DP, Bryan YG. Microencapsulated phase change material suspensions for heat transfer in spacecraft thermal systems. J Spacecr Rockets 1996; 33: 278–284.

[41] Pesaran AA. Battery thermal models for hybrid vehicle simulations. J Power Sources 2002; 110: 377–382.

[42] Fang YT, Kuang SY, Gao XN, Mang ZG. Preparation and characterization of novel nanoencapsulated phase change materials. Energ Convers Manage 2008; 49: 3704–3707.

[43] Malik M, Dincer I, Rosen MA. Review on use of phase change materials in battery thermal management for electric and hybrid electric vehicles. Int J Energ Res 2016; 40: 1011–1031.

[44] Rao Y, Dammel F, Stephan P, Lin GP. Flow frictional characteristics of microencapsulated phase change material suspensions flowing through rectangular minichannels. Sci China Ser E 2006; 49: 445-456.

[45] Yan JJ, Li K, Chen HD, Wang QS, Sun JH. Experimental study on the application of phase change material in the dynamic cycling of battery pack system. Energ Convers Manage 2016; 128: 12–19.

[46] Wang C, Zhang GQ, Meng LK, Li XX, Situ WF, Lv YF, Rao M. Liquid cooling based on thermal silica plate for battery thermal management system. Int J Energ Res 2017; 41: 2468–2479.

[47] Cengel Y, Ghajar A, Heat and Mass Transfer: Fundamentals & Applications, McGraw-Hill, New York, NY, USA, 4th edition, 2011.